Electron vortices in photoionization by a pair of elliptically polarized attosecond pulses

Meng Li (李 猛)[1,2], Guizhong Zhang (张贵忠)[1,*], Tianqi Zhao (赵天琪)[1], Xin Ding (丁 欣)[1], and Jianquan Yao (姚键铨)[1]

[1]*College of Precision Instrument and Optoelectronics Engineering, Tianjin University, Tianjin 300072, China*
[2]*Civil Aviation Meteorological Institute, Key Laboratory of Operation Programming & Safety Technology of Air Traffic Management, Civil Aviation University of China, Tianjin 300300, China*
**Corresponding author: johngzhang@tju.edu.cn*

Received September 12, 2017; accepted November 1, 2017; posted online November 16, 2017

The photoionization by two elliptically polarized, time delayed attosecond pulses is investigated to display a momentum distribution having the helical vortex or ring structures. The results are obtained by the strong field approximation method and analyzed by the pulse decomposition. The ellipticities and time delay of the two attosecond pulses are found to determine the rotational symmetry and the number of vortex arms. For observing these vortex patterns, the energy bandwidth and temporal duration of the attosecond pulses are ideal.

OCIS codes: 020.2649, 020.0020, 260.3230.
doi: 10.3788/COL201715.120202.

When an atom or a molecule is subject to an intense laser field, ionization or dissociation will generally occur, and the direct outcome of the ionization process is that the dislodged electron will manifest a spectrum of either momentum or energy. Therefore, momentum distributions[1], including the angular distribution of momentum of the ionized electron, are extensively investigated in the realm of atomic, molecular, and optical physics[2–4]. Pertaining to the ionizing electric field of the strong laser pulse, a variety of pulse combinations have been deployed: single color or two colors[5–7], linearly or circularly polarized[8–11], few-cycle or many cycles[12,13], and infrared or ultraviolet (UV)[14,15].

A few years ago, Ramsey-type interference[16] of laser-induced electron wavepackets was found to show a totally new feature: vortex-shaped momentum distribution[17,18] when two circularly polarized[19,20] weak to intermediate intensity laser pulses were used in atomic or molecular ionization. The novel finding is that the induced momentum distribution of the ionized electron on the plane of the laser polarization showed spiral structure or vortex-shaped momentum distribution[21–24]. The counter-rotating circularly polarized pulses would lead to a spiral momentum feature, while co-rotating laser pulses produced no vortex momentum at all. More importantly, this kind of vortex momentum distribution has been confirmed experimentally using argon atoms[25]. It was also found that fairly small carrier frequency, fairly long pulse duration, and improper combination of pulse parameters showed little vortex momentum shape.

In 2007, the semiclassical dynamics of electron wavepackets were investigated, carrying orbital angular momentum[26]. Djiokap *et al.*[17] numerically studied the helium photoionization by oppositely circularly polarized, time delayed attosecond pulses. Their finding was that two-start photoelectron momentum distribution was induced for proper left/right or right/left laser helicities. Then, the single ionization of the helium atom subject to circularly polarized laser pulses were numerically studied[27]. Vortex momentum patterns of zero-start, one-start, three-start, and four-start were discovered for a UV carrier frequency of 15 eV and intensity of 10^{12} W/cm^2. Yuan *et al.*[28] theoretically investigated the photoelectron momentum distribution of the molecular helium ion by bichromatic circularly polarized attosecond UV laser pulses. They discovered that co- and counter-rotating pulses could induce spiral momentum distribution. This is the first report, to the best of our knowledge, on vortex momentum formation in a molecule. In 2017, Pengel *et al.*[25] experimentally measured a sequence of two counter-rotating circularly polarized femtosecond laser pulses that would lead to electron vortices with c_4 and c_6 rotational symmetry[17] in the photoionization of the potassium atom. Their experimental results were also compared with numerical simulation. The agreement is excellent.

In this Letter, we investigate a special kind of electron vortices in photoionization by a pair of time delayed elliptically polarized attosecond pulses[29,30]. In the polarization plane, these special momentum distributions exhibit complex mixing vortices that vary by the ellipticity of two pulses, whose signs and absolute values determine the handedness and shape of the special vortex patterns, respectively. The large bandwidth of attosecond pulses is required for observation. Furthermore, our predicted electron vortices display progressive features of right–left and left–right photoionizations, demonstrating an unusual kind of control on photoelectrons in the attosecond time scale.

In our view, the photoionization by a pair of polarized attoseconds is a process of interaction between the tunnel and multi-photon ionization. The ellipticities and time delay of two polarized attosecond pulses are the most

important parameters to determine the electron vortex pattern. A pair of elliptically polarized pulses, time delayed by τ, interacts with the hydrogen atom in the ground state with the same frequency ω_i and pulse envelope $F_i(t)$, differing in the ellipticity η_i and carrier envelope phases (CEPs) θ_i:

$$\begin{aligned} F(t) &= F_1(t) + F_2(t-\tau), \\ F_i(t) &= I_0\left[\frac{1}{(1+\eta_i^2)^{0.5}}\cos(\omega_i t+\theta_i)\hat{x}\right. \\ &\quad \left.+\frac{\eta_i}{(1+\eta_i^2)^{0.5}}\sin(\omega_i t+\theta_i)\hat{y}\right] \\ &\quad \times \cos^2(\pi t/T) \quad (-T/2 < t < T/2, i = 1, 2). \end{aligned} \tag{1}$$

The polarization state of the ith pulse associates with the ellipticity η_i; if $\eta_i = 1$, the artificial attosecond pulse is circularly polarized; if $\eta_i = 0$, it is linearly polarized. Elliptical polarization indicates the intermediate state of the polarized attosecond pulse in the range of $|\eta_i| < 1$. The linear and circular polarization degrees of the ith pulse are $\zeta_i = \frac{1-\eta_i^2}{1+\eta_i^2}$ and $\xi_i = \frac{2\eta_i}{1+\eta_i^2}$, where $\zeta_i^2 + \xi_i^2 = 1$. We compute the photoionization spectrum for carrier frequency $\omega = 0.147$ a.u. and an electric field $I_0 = 10^{14}$ W/cm^2. $T = n_p\frac{2\pi}{\omega} = 2998$ as is the total pulse duration for $n_p = 3$ optical cycles. The temporal envelope in each pulse can be expressed as $\cos^2(\pi t/T)$, where T is the pulse duration. The predicted vortices involve the processes of single-photon ionization. Thus, lower intensity is required for the vortex patterns to occur.

Without considering the coulomb interaction between the nucleus and the ionized electron[31], the strong field approximation (SFA) is deployed to investigate the photoelectron momentum spectra induced by a pair of time delayed elliptically polarized attosecond pulses. Theoretically speaking, the numerical solution to the time-dependent Schrodinger equation, including the interaction between the electron and the applied laser field, is the only correct way to analyze the strong field process in atoms and molecules. However, the only doable systems are limited to two electrons with six degrees of freedom, due mainly to the computer ability nowadays. On the other hand, approximate methods, which are able to capture the essential physics, while the numerical computation is feasible, turn out to be the workhorse in the realm of strong field physics.

The probability amplitude of the photoionized electron in the continuum states with momentum is

$$f(\vec{p}) = -i\int_{-\infty}^{\infty} \mathrm{d}t' \exp\left[i\int_{t'}^{\infty}\mathrm{d}t''\left[I_p + \frac{[\vec{p}+\vec{A}]^2}{2}\right]\right]\vec{d}(\vec{p})\cdot\vec{E}, \tag{2}$$

where $\vec{A}$ and $\vec{E}$ indicate the vector potential and the total electric fields, respectively. I_p is the ionization threshold of the hydrogen atom (0.5 a.u.). For hydrogen, the transition dipole moment $\vec{d}(\vec{p})$ can be expressed as

$$\vec{d}(\vec{p}) = \frac{2^{3.5}\times(2I_p)^{5/4}}{\pi}[\vec{p}/(\vec{p}^2 + 2I_p)^3]. \tag{3}$$

Archimedean spirals can describe the maxima of the vortices. For the elliptically polarized pulse, the intrapulse time delay and ellipticity control the energy spectrum of the spiral lines. During nonperturbative interaction, the population dynamics of the first pulse controls the initial conditions of the second pulse. The initially created electron wave packet generates an energy-dependent $-\tau E/\hbar$, in which E expresses the electron excess energy. In Fig. 1(a), if $\eta_1 = 1$, and $\eta_2 = -1$, a pair of elliptically polarized attosecond pulses is shown as a right-handed circularly polarized pulse, followed by the second left-handed circularly polarized pulse. Ionization with a right-handed circularly polarized pulse proceeds via the $|s,0\rangle \to |p,-1\rangle \to |d,-2\rangle \to |f,-3\rangle \to |g,-4\rangle$ states, where $|l,m\rangle$ describes the angular part of the wave function. $|s,0\rangle$ describes the ground atomic bound, while $|p,-1\rangle$ is the continuum (positive energy) electron state having the orbital quantum number $l = 1$, and the magnetic quantum number $m = 1$. One photon with helicity one is absorbed, and angular momentum projection on the quantization axis, which is perpendicular to the laser polarization plane, is conserved.

Due to the time delay between two pulses, the first electron wave packet will obtain a phase of $-\tau E/\hbar$ when the first one is generated. In the perturbative limit, the $|s,0\rangle$ ground state remains unchanged by the first pulse. Thus, ionization with the second left circularly polarized pulse proceeds via the $|s,0\rangle \to |p,1\rangle \to |d,2\rangle \to |f,3\rangle \to |g,4\rangle$ states.

Thus, the electron wave packet results in the coherent superposition states with quantum numbers $m = \pm 4$:

$$|\psi_8\rangle \propto e^{-i\tau E/\hbar}|f,-4\rangle + |f,4\rangle. \tag{4}$$

The interference of two states $|f,-4\rangle$ and $|f,4\rangle$ exhibits c_8 rotational symmetry[17].

For

$$\begin{cases} -1 < \eta_1, \eta_2 < 1 \\ \eta_1 \cdot \eta_2 < 0 \\ \eta_1 = -\eta_2 \end{cases}, \tag{5}$$

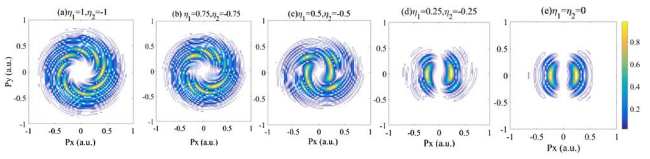

Fig. 1. Photoelectron momentum distributions in the polarization plane for ionization of hydrogen by right–left circularly polarized attosecond pulses with the ellipitcity (a) $\eta_1 = 1$, $\eta_2 = -1$, (b) $\eta_1 = 0.75, \eta_2 = -0.75$, (c) $\eta_1 = 0.5$, $\eta_2 = -0.5$, (d) $\eta_1 = 0.25$, $\eta_2 = -0.25$, (e) $\eta_1 = 0$, $\eta_2 = 0$, which are delayed in time by 2478 as.

due to the unequal energy distribution of the elliptically polarized attosecond pulses in the polarization plane, the pulse energy can be decomposed into a circularly polarized pulse $F_i^{\rm cir}$ and a linearly polarized pulse $F_i^{\rm lin}$, which are presented as

$$\begin{aligned} F_i(t) &= F_i^{\rm lin}(t) + F_i^{\rm cir}(t) \quad (-T/2 < t < T/2), \\ F_i^{\rm lin}(t) &= E_0\left[\frac{1-\eta_i}{(1+\eta_i^2)^{0.5}}\cos(\omega_i t+\theta_i)\hat{x}\right] \\ &\quad \times \cos^2(\pi t/T) \quad (-T/2 < t < T/2), \\ F_i^{\rm cir}(t) &= E_0\frac{\eta_i}{(1+\eta_i^2)^{0.5}}[\cos(\omega_i t+\theta_i)\hat{x} + \sin(\omega_i t+\theta_i)\hat{y}] \\ &\quad \times \cos^2(\pi t/T) \quad (-T/2 < t < T/2). \end{aligned} \tag{6}$$

A paired of time delayed linearly polarized pulsed can be considered special elliptically polarized attosecond pulses of $\eta_1 = 0, \eta_2 = 0$. Shown as Fig. 1(e), the ionization spectrum of a pair of the linearly polarized pulses cannot exhibit the vortex shape but have the characteristic of rotational symmetry, which contributes to the c_2 rotation symmetry for the final ionization spectrum pattern of the elliptically polarized attosecond pulses. On the other hand, the photoelectron momentum distribution with two time delayed counter-rotating circularly polarized pulses exhibits the c_8 rotational symmetry and has eight vortex arms according to the above discussion. However, because the overlapping of the c_8 pattern and c_2 pattern is the c_2 pattern, for the elliptically polarized attosecond pulses, the photoelectron momentum distribution exhibits c_2 symmetry and has 2–8 vortex arms, described as Fig. 1. The number of vortex arms varies with the ellipticity η. With the increase of $|\eta|$, the number of vortex arms also increases.

For instance, if $\eta_1 = -0.5$, $\eta_2 = 0.5$, the elliptically polarized attosecond pulses can be divided into a circularly polarized pulse and a linearly polarized pulse. The circularly polarized pulse determines that the largest number of the vortex arms is eight. The linearly polarized pulse determines that the momentum distribution spectrum exhibits c_2 rational symmetry. However, because the equal linearly polarized pulse effects the shape of the vortex arms seriously, the vortex arms begin to fuse along the rotational direction and enhance with the decrease of $|\eta_1|$ and $|\eta_2|$, shown as Fig. 1(c). The vortex arms fuse and are gradually separated by one gap, which applies to all of the momentum distribution with a pair of time delayed equal ellipticity elliptically polarized attosecond pulses. For $\eta_1 = 0.25$, $\eta_2 = -0.25$, it can be seen that the momentum distribution spectrum has evolved into a c_2 rotation symmetry with two vortex arms, which is similar to the spectrum pattern ionized by a pair of the linearly polarized pulses.

For the case of a pair of unequal elliptically polarized attosecond pulses,

$$\begin{cases} -1 < \eta_1, \eta_2 < 1 \\ \eta_1 \cdot \eta_2 < 0 \\ \eta_1 \neq -\eta_2 \end{cases}. \tag{7}$$

The elliptically polarized attosecond pulses are also considered as the addition of a circularly polarized pulse and a linearly polarized pulse. However, because the ellipticity of two elliptically polarized attosecond pulses are unequal, the ionization momentum distribution spectrum exhibits a mixed state of two pairs of time delayed elliptically polarized attosecond pulses with different η. The ionization spectrum for $\eta_1 = -1, \eta_2 = 0.5$ approaches the mixed state of the ones for $\eta_1 = -1$, $\eta_2 = 1$ and $\eta_1 = -0.5$, $\eta_2 = 0.5$, shown as Fig. 2. In our view, for simplifying calculations, a pair of unequal elliptically polarized attosecond pulses can be decomposed into a pair of equal elliptically polarized attosecond pulses $F_i^{\rm eq}(t)$ and a linearly polarized pulse $F_i^{\rm lin}(t)$, which can be translated into

$$\begin{aligned} F(t) &= F_i^{\rm eq}(t) + F_i^{\rm lin}(t) \qquad (i = 1, 2), \\ F_1^{\rm eq}(t) &= F_1(t) + F_1(t-\tau), \\ F_1^{\rm lin}(t) &= F_2(t-\tau) - F_1(t-\tau), \\ F_2^{\rm eq}(t) &= F_2(t) + F_2(t-\tau), \\ F_2^{\rm lin}(t) &= F_1(t) - F_2(t). \end{aligned} \tag{8}$$

The number of the vortex arms and the shape of the ionization momentum distribution mainly depend on the equal elliptically polarized attosecond pulses $F_i^{\rm eq}(t)$. The linearly polarized pulse $F_i^{\rm lin}(t)$ affects the vortex pattern slightly, because it only has one polarization direction. For instance, the ionization spectrum with $\eta_1 = -0.5, \eta_2 = 0.25$ has six vortex arms between the vortex arm numbers of the one with $\eta_1 = -0.5, \eta_2 = 0.5$ and $\eta_1 = -0.25$, $\eta_2 = 0.25$. It exhibits a mixed state of two cases.

Experimental observation of the vortex patterns in the photo-electron momentum distributions requires a pair of oppositely elliptically polarized attosecond pulses with low intensity, but with control of the time delay and the relative CEP between two pulses. For the case of $\eta_1 = 1, \eta_2 = 1$, the photoelectron momentum distributions exhibit a form similar to Newton's rings, based upon Ramsey interference of the two electronic wave packets.

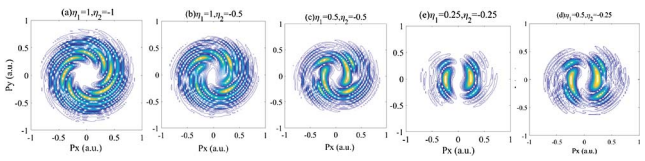

Fig. 2. Photoelectron momentum distributions in the polarization plane for ionization of H by right–left circularly polarized attosecond pulses with the ellipitcity (a) $\eta_1 = 1$, $\eta_2 = -1$, (b) $\eta_1 = 1$, $\eta_2 = -0.5$, (c) $\eta_1 = 0.5$, $\eta_2 = -0.5$, (d) $\eta_1 = 0.25$, $\eta_2 = -0.25$, (e) $\eta_1 = 0.25$, $\eta_2 = -0.25$, which are delayed in time by 2478 as.

Ionization with a pair of right-handed elliptically polarized attosecond pulses proceeds via the same pathway $|s,0\rangle \rightarrow |p,-1\rangle \rightarrow |d,-2\rangle \rightarrow |f,-3\rangle \rightarrow |g,-4\rangle$ state. Therefore, taking a phase of $-\tau E/\hbar$ into consideration, the wave packet function is composed of the contributions:

$$|\psi\rangle \propto e^{-i\tau E/\hbar}|g,-4\rangle + |g,-4\rangle. \tag{9}$$

For the case of

$$\begin{cases} -1 < \eta_1, \eta_2 < 1 \\ \eta_1 \cdot \eta_2 > 0 \end{cases}, \tag{10}$$

owing to the difference of the ellipticity η_1 and η_2, Newton's rings exhibit different characteristics. If $\eta_1 = \eta_2$, the momentum spectra are regular and the symmetry rings have two gaps along the radial direction in the momentum space. If $\eta_1 \neq \eta_2$, the ones exhibit irregular rings that have two misplaced gaps, because two time delayed elliptically polarized attosecond pulses have different energies in the polarization plane for the photoionization process [displayed as Fig. 3(c)]. The asymmetry of the ring pattern varies with the difference between η_1 and η_2.

For simplifying the process, two time delayed left-handed (or right-handed) pulses can also be regarded as a pair of equal elliptically polarized attosecond pulses combined with a single linearly polarized attosecond pulse, which is expressed as Eq. (1). The part of elliptically polarized attosecond pulses still contributes to the main shape and number of the "Newton's rings". But, the size of the gaps in the ionization momentum distribution depends on the linearly polarized attosecond pulse. As shown in Fig. 3, for $\eta_1 = 0.5$, $\eta_2 = 0.25$, the ionization spectrum pattern exhibits three asymmetry rings with two gaps. In contrast, the ones with $\eta_1 = 0.5$, $\eta_2 = 0.5$ exhibit two symmetry rings. But, due to the ellipticity being closer to zero, the momentum distribution with $\eta_1 = 0.25$, $\eta_2 = 0.25$ has several symmetry curves, which shows the characteristics of the ionization spectrum with linear pulses.

Additionally, the ellipticity $\eta = 0$ is a special case, where the elliptically polarized attosecond pulses are evolved into a linearly polarized pulse. For $\eta_1 = -0.5$, $\eta_2 = 0$, as well as $\eta_1 = -1$, $\eta_2 = 0$, a pair of elliptically polarized attosecond pulses is regarded as a right-handed pulse following a linearly polarized pulse. Ionization with two pulses only proceeds only via the pathway $|s,0\rangle \rightarrow |p,-1\rangle \rightarrow |d,-2\rangle \rightarrow |f,-3\rangle \rightarrow |g,-4\rangle$ state. Thus, the momentum spectrum does not exhibit the characteristics of the ring and vortices, shown as Fig. 4.

For a pair of opposite elliptically polarized attosecond pulses, the ionization momentum distribution pattern associates with the ellipticity, which determines the number of vortex arms and the rational symmetry. For the case that the linearly polarized pulse decomposition of the elliptically polarized attosecond pulses exceeds a threshold, the photoionization of the circularly polarized pulse decomposition is covered, and the vortex momentum spectrum cannot be displayed.

Our numerical results for the SFA for two oppositely elliptically polarized few-cycle attosecond pulses are displayed in Fig. 5, where we plot the photoelectron momentum distributions in the polarization plane for various time delays and ellipticities. Figs. 5(a), 5(b), and 5(c) are for a pair of common elliptically polarized attosecond pulses with $\eta_1 = 0.5$, $\eta_2 = -0.5$. It can be seen that the

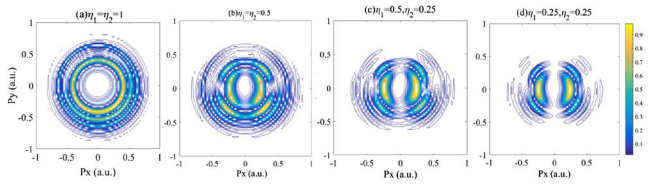

Fig. 3. Photoelectron momentum distributions in the polarization plane for ionization of H by right–right circularly polarized attosecond pulses with the ellipitcity (a) $\eta_1 = \eta_2 = 1$, (b) $\eta_1 = \eta_2 = 0.5$, (c) $\eta_1 = 0.5$, $\eta_2 = 0.25$, (d) $\eta_1 = \eta_2 = 0.25$, which are delayed in time by 2478 as.

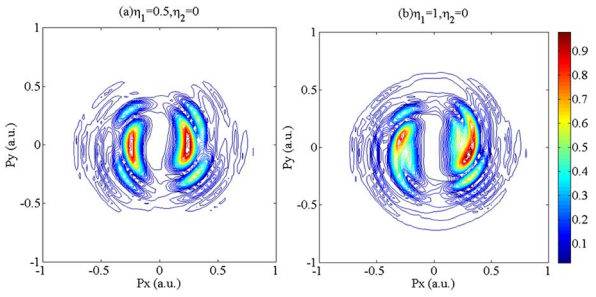

Fig. 4. Photoelectron momentum distributions in the polarization plane for ionization of H by a linearly polarized attosecond pulse and a circularly polarized attosecond pulse with the ellipitcity (a) $\eta_1 = 0.5$, and (b) $\eta_1 = 1$, which are delayed in time by 2478 as.

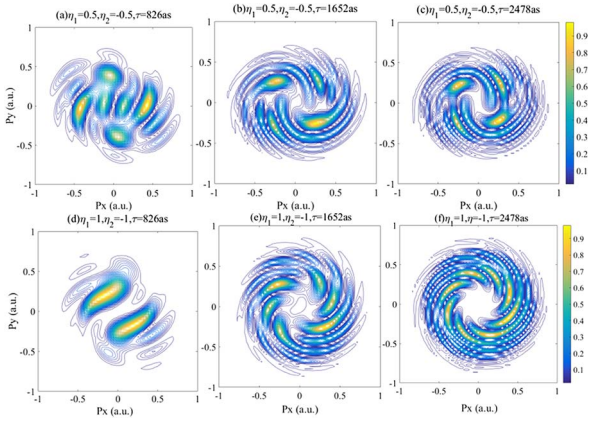

Fig. 5. Photoelectron momentum distributions in the polarization plane for ionization of H by a right–left elliptically polarized attosecond pulse with the ellipitcity (a)–(c) $\eta_1 = 0.5$, $\eta_2 = -0.5$, and (d)–(f) $\eta_1 = 1$, $\eta_2 = -1$, delayed in time by (a) and (d) 826 as, (b) and (e) 1652 as, and (c) and (f) 2478 as.

time delay impacts the vortex pattern. For a smaller time delay, such as $\tau = 826$ as, two elliptically polarized attosecond pulses are close to each other, which effects the form of the vortex in the photoionization. Therefore, the vortex pattern is vague with the thick vortex arms in the photoelectron momentum distributions. But, for $\tau = 1652$ as, and $\tau = 2478$ as, enough time delay ensures the well-defined vortex pattern, which exactly shows the C_2 rational with six vortex arms. On the other hand, in Figs. 5(d), 5(e), and 5(f), we display the photoelectron momentum distributions for a pair of opposite circularly polarized attosecond pulses. In addition to the result demonstrated in the case of $\eta_1 = 0.5$, $\eta_2 = -0.5$, one can also observe that the time delay effects the number of the vortex arms. For $\tau = 1652$ as, the number of vortex arms is six, while for $\tau = 2478$ as, the one is eight. Moreover, for the same time delay, smaller ellipticity η easily exhibits the characteristics of the vortex pattern. For $\eta_1 = 1$, $\eta_2 = -1$, if the time delay is $\tau = 826$ as, the vortex disappears completely, shown as Fig. 5(d), while for $\eta_1 = 0.5$, $\eta_2 = -0.5$, six thick vortex arms can also be discerned. Vortices in the probability distribution depend on the time delay and ellipticity.

In conclusion, a special photoionization with a pair of time delayed elliptically polarized attosecond pulses is investigated by the SFA. As demonstrated in the momentum distribution pattern, the rational symmetry and the vortex line number are sensitive to the time delay and ellipticity of two elliptically polarized attosecond pulses. The ionization pathways were selected by the field strength via the population dynamics and the laser polarization via selection rules. In our strategy, an elliptically polarized attosecond pulse with varying ellipticity is regarded as an addition of the circularly and linearly polarized attosecond pulses for simplifying the calculation. The final momentum distribution by a pair of elliptically polarized attosecond pulses exhibits a mixed state of the ones generated by the circularly and linearly polarized attosecond pulses. The signs of the ellipiticity determine the shape (vortex or ring) of the momentum distribution. In addition, the time delay can also affect the characteristics of the vortex pattern. Experimental observation of these vortex patterns in the photoelectron momentum distributions requires a pair of oppositely elliptically polarized attosecond pulses with low intensity but with control of the time delay between two pulses. In the extreme UV, generation of the circularly polarized harmonics energy regime has recently been achieved[32]. Reaction microscope techniques and velocity map imaging are used to measure the momentum spectrum. The sensitivity of the vortex-shaped patterns to the parameters of the pair of attosecond pulses makes them an ideal method of timing ultrafast processes and of characterizing these pulses.

This work was supported by the National Natural Science Foundation of China (Nos. 11674243 and 11674242) and the Fundamental Research Funds for the Central Universities (No. 3122016D029).

References

1. M. Hentschel, R. Kienberger, C. Spielmann, G. A. Reider, N. Milosevic, T. Brabec, P. Corkum, U. Heinzmann, M. Drescher, and F. Krausz, Nature **414**, 509 (2001).
2. E. Goulielmakis, V. S. Yakovlev, A. L. Cavalieri, M. Uiberacker, V. Pervak, A. Apolonski, R. Kienberger, U. Kleineberg, and F. Krausz, Science **317**, 769 (2007).
3. H. Du, L. Luo, X. Wang, and B. Hu, Opt. Express **20**, 9713 (2012).
4. Q. Wang, Y. Zhang, Z. Wang, J. Ding, Z. Liu, and B. Hu, Chin. Opt. Lett. **14**, 110201 (2016).
5. M.-H. Xu, L.-Y. Peng, Z. Zhang, Q. Gong, and X.-M. Tong, Phys. Rev. Lett. **107**, 183001 (2011).
6. M. Li, J.-W. Geng, M.-M. Liu, X. Zheng, L.-Y. Peng, Q. Gong, and Y. Liu, Phys. Rev. A **92**, 013416 (2015).
7. J.-W. Geng, W.-H. Xiong, X.-R. Xiao, L.-Y. Peng, and Q. Gong, Phys. Rev. Lett. **115**, 193001 (2015).
8. L. Y. Peng, E. A. Pronin, and A. F. Starace, New J. Phys. **10**, 025030 (2008).
9. P.-L. He, C. Ruiz, and F. He, Phys. Rev. Lett. **116**, 203601 (2016).
10. S.-S. Wei, S.-Y. Li, F.-M. Guo, and Y.-J. Yang, Phys. Rev. A **87**, 063418 (2013).
11. C. Figueira de Morisson Faria, H. Schomerus, X. Liu, and W. Becker, Phys. Rev. A **69**, 043405 (2004).
12. L.-Y. Peng and A. F. Starace, Phys. Rev. A **76**, 043401 (2007).
13. N. Douguet, A. N. Grum-Grzhimailo, E. V. Gryzlova, E. I. Staroselskaya, J. Venzke, and K. Bartschat, Phys. Rev. A **93**, 033402 (2016).
14. S. X. Hu, Phys. Rev. Lett. **111**, 123003 (2013).
15. A. N. Grum-Grzhimailo, A. D. Kondorskiy, and K. Bartschat, J. Phys. B: At. Mol. Opt. Phys. **39**, 4659 (2006).
16. N. F. Ramsey, Phys. Rev. **78**, 695 (1950).
17. M. N. Djiokap, S. X. Hu, L. B. Madsen, N. L. Manakov, A. V. Meremianin, and A. F. Starace, Phys. Rev. Lett. **115**, 113004 (2015).
18. M. Harris, C. A. Hill, and J. M. Vaughan, Opt. Commun. **106**, 161 (1994).
19. K. Zhai, Z. Li, H. Xie, C. Jing, G. Li, B. Zeng, W. Chu, J. Ni, J. Yao, and Y. Cheng, Chin. Opt. Lett. **13**, 050201 (2015).
20. Y. Xie, Y. Yang, L. Han, Q. Yue, and C. Guo, Chin. Opt. Lett. **14**, 122601 (2016).
21. I. Bialynicki-Birula, Z. Bialynicka-Birula, and C. Sliwa, Phys. Rev. **A61**, 032110 (2000).
22. S. J. Ward and J. H. Macek, Phys. Rev. A **90**, 062709 (2014).
23. J. H. Macek, J. B. Sternberg, S. Y. Ovchinnikov, and J. S. Briggs, Phys. Rev. Lett. **104**, 033201 (2010).
24. J. M. Feagin, J. Phys. B **44**, 011001 (2011).
25. D. Pengel, S. Kerbstadt, D. Johannmeyer, L. Englert, T. Bayer, and M. Wollenhaupt, Phys. Rev. Lett. **118**, 053003 (2017).
26. K. Y. Bliokh, Y. P. Bliokh, S. Savel'ev, and F. Nori, Phys. Rev. Lett.1 **99**, 190404 (2007).
27. J. M. Ngoko Djiokap, A. V. Meremianin, N. L. Manakov, S. X. Hu, L. B. Madsen, and A. F. Starace, Phys. Rev. A **94**, 013408 (2016).
28. K.-J. Yuan, S. Chelkowski, and A. D. Bandrauk, Phy. Rev. A **93**, 053425 (2016).
29. K. Zhai, Z. Li, H. Xie, C. Jing, G. Li, B. Zeng, W. Chu, J. Ni, J. Yao, and Y. Cheng, Chin. Opt. Lett. **13**, 050201 (2015).
30. Y. Xie, Y. Yang, L. Han, Q. Yue, and C. Guo, Chin. Opt. Lett. **14**, 122601 (2016).
31. P. L. He, N. Takemoto, and F. He, Phys. Rev. A **91**, 063413 (2015).
32. O. Kfir, P. Grychtol, E. Turgut, R. Knut, D. Zusin, D. Popmintchev, T. Popmintchev, H. Nembach, J. M. Shaw, A. Fleischer, H. Kapteyn, M. Murnane, and O. Cohen, Nat. Photon. **9**, 99 (2014).